High-Frame-Rate Speckle-Tracking Echocardiography

Philippe Joos, Jonathan Porée, Hervé Liebgott, Didier Vray, Mathilde Baudet, Julia Faurie, François Tournoux, Guy Cloutier, Barbara Nicolas, and Damien Garcia

***Abstract*— Conventional echocardiography is the leading modality for noninvasive cardiac imaging. It has been recently illustrated that high-frame-rate echocardiography using diverging waves could improve cardiac assessment. The spatial resolution and contrast associated with this method are commonly improved by coherent compounding of steered beams. However, owing to fast tissue velocities in the myocardium, the summation process of successive diverging waves can lead to destructive interferences if motion compensation (MoCo) is not considered. Coherent compounding methods based on MoCo have demonstrated their potential to provide high-contrast B-mode cardiac images. Ultrafast speckle-tracking echocardiography (STE) based on common speckle-tracking algorithms could substantially benefit from this original approach. In this paper, we applied STE on high-frame-rate B-mode images obtained with a specific MoCo technique to quantify the 2-D motion and tissue velocities of the left ventricle. The method was first validated *in vitro* and then evaluated *in vivo* in the four-chamber view of 10 volunteers. High-contrast high-resolution B-mode images were constructed at 500 frames/s. The sequences were generated with a Verasonics scanner and a 2.5-MHz phased array. The 2-D motion was estimated with standard cross correlation combined with three different subpixel adjustment techniques. The estimated *in vitro* velocity vectors derived from STE were consistent with the expected values, with normalized errors ranging from 4% to 12% in the radial direction and from 10% to 20% in the cross-range direction. Global longitudinal strain of the left ventricle was also obtained from STE in 10 subjects and compared to the results provided by a clinical scanner: group means were not statistically different (p value = 0.33). The *in vitro* and *in vivo* results showed that MoCo enables preservation of the myocardial speckles and in turn allows high-frame-rate STE.**

***Index Terms*— Cardiac imaging, diverging waves, high-frame-rate echocardiography, motion compensation (MoCo), speckle-tracking echocardiography (STE), ultrafast ultrasound.**

I. Introduction

ECHOCARDIOGRAPHY is one of the most widespread modalities for cardiovascular imaging due to its high temporal resolution and low cost, because it is a safe real-time diagnostic imaging modality [1]. Speckle-tracking echocardiography (STE) is a quantitative method for assessing the dynamics of cardiac motion. It allows the measurement of myocardial velocities and deformations in the short-axis and apical views and provides valuable information on cardiac synchrony and function [2]. When STE is used to derive strains and strain rates, this technique is also referred to as "strain imaging" [3]. STE is now recognized as a quantitative key tool in clinical cardiac research. STE algorithms generally use a block-matching approach to track the speckles in a sequence of 2-D B-mode (grayscale) images [4]. In the current clinical practice, it is admitted that a frame rate of 50–80 frames/s returns optimal conditions for speckle tracking in the resting heart beating at ∼70 bpm [5]. In some situations, such as for the evaluation and management of coronary artery disease, it can be recommended to increase the heart rate during an echocardiographic examination, i.e., perform a stress echocardiography [6]. In a stressed myocardium, the mechanical events become shorter; the acquisition frame rate should thus be increased (probably proportionally) with the heart rate (up to 120–140 bpm) [5]. Acquiring the whole left ventricular myocardium at such high frame rates is challenging with the conventional imaging systems. For this reason, no consensus has been reached about the incorporation of STE in routine stress echocardiography. Stress echocardiography could thus benefit from high-frame-rate ultrasound imaging (100–500 frames/s) [7], [8].

Several techniques have been proposed in the past few years to increase frame rate in transthoracic cardiac ultrasound imaging while keeping high-quality images. Transmit schemes based on focused or unfocused beams have been introduced. In the multiline transmit (MLT) technique, several

Manuscript received January 13, 2018; accepted February 19, 2018. Date of publication February 27, 2018; date of current version May 7, 2018. This work was supported in part by the Fonds de Recherche du Québec-Nature et Technologies, in part by the LABEX Center Lyonnais d'Acoustique, in part by ANR-10 et Simulation (PRIMES) under Grant ANR-10-LABX-0063, and in part by Investissements d'Avenir under Grant ANR-11-IDEX-0007. The work of H. Liebgott and P. Joos was supported by Région Rhône-Alpes under Grant Explora'Pro and Explora'Doc. The work of D. Garcia was supported by the Natural Sciences and Engineering Research Council of Canada under Grant RGPAS-477914-2015 and Grant RGPIN-04217-2015. The work of D. Garcia and G. Cloutier was supported by the Fonds de Recherche du Québec-Nature et Technologies under Grant 2016-PR-189822. The work of M. Baudet was supported by the French Federation of Cardiology. *(Corresponding author: Damien Garcia.)*

P. Joos, H. Liebgott, D. Vray, and B. Nicolas are with Univ Lyon, INSA-Lyon, Université Claude Bernard Lyon 1, UJM-Saint Étienne, CNRS, Inserm, CREATIS UMR 5220, U1206, 69361 Lyon, France.

J. Porée and J. Faurie are with the Laboratory of Biorheology and Medical Ultrasonics, University of Montreal Hospital Research Center, Montreal, QC H2X 0A9, Canada.

M. Baudet and F. Tournoux are with the Echocardiographic Laboratory, University of Montreal Hospital, Montreal, QC H2W 1T8, Canada.

G. Cloutier is with the Laboratory of Biorheology and Medical Ultrasonics, University of Montreal Hospital Research Center, Montreal, QC H2X 0A9, and also with the Department of Radiology, Radio-Oncology and Nuclear Medicine, the Institute of Biomedical Engineering, University of Montreal, Montreal, QC H3T 1J4, Canada.

D. Garcia is with Univ Lyon, INSA-Lyon, Université Claude Bernard Lyon 1, UJM-Saint Étienne, CNRS, Inserm, CREATIS UMR 5220, U1206, 69361 Lyon, France. He was with the Research Center of the University of Montreal Hospital, Montreal, QC H2X 0A9, Canada, and also with the Department of Radiology, Radio-Oncology and Nuclear Medicine, University of Montreal, Montreal, QC H3T 1J4, Canada (e-mail: garcia.damien@gmail.com).

Digital Object Identifier 10.1109/TUFFC.2018.2809553

focused beams are transmitted into different directions [9]. Combined with multiline acquisition, MLT frame rate can be further increased [10]. MLT-based tissue Doppler imaging at >200 frames/s was recently reported [11]. Ultrafast cardiac ultrasound imaging is also possible with diverging waves [12]–[14]. To preserve contrast and spatial resolution in unfocused wave imaging, coherent compounding of images derived from different steering-angle transmits is essential since the individual images are of poor quality. Coherent compounding corrects the phase delays related to the transmit and receive travel times. It improves the image quality of motionless or slow-moving tissues. However, if the motion of fast-moving scatterers is neglected, it may cause destructive interferences and, in turn, degrade contrast and resolution [15], [16]. Indeed, large motions can generate substantial phase delays, thus producing noncoherent summation. Consequently, a traditional compounding approach is not adapted to cardiac imaging, especially under pharmacological stress or physical exertion. The integration of motion compensation (MoCo) in the compounding process has been shown to ensure coherent summation and thus improve the image quality significantly. MoCo is based on the estimation of axial [16] or 2-D [17] motion between the successive tilted images. The signals are then rephased before being summed coherently. It has been shown in [14] that radial (axial) motion only needs to be compensated in phased-array cardiac imaging since the cross-range resolution is low compared with that of the radial resolution. It has also been demonstrated in the same study that a triangle transmit sequence (i.e., steering angles increasing then decreasing linearly) is more efficient than linear or alternate transmission strategies for MoCo based on Doppler estimation. The triangle sequence has the advantage to sum the main lobes coherently and the side lobes incoherently. To apply MoCo, the motion is assumed constant during N successive transmits, providing one tissue Doppler image: one high-quality compound image is then obtained by summing the N motion-compensated complex envelopes.

Speckle tracking is a suitable method for myocardium displacement measurement [4]. This technique, based on the local conservation of the speckle patterns, cannot be applied if artifacts or poor image quality compromise speckle recognition from one frame to the next one. As illustrated in the human left ventricle [14], coherent compounding can produce major signal losses if MoCo is not integrated. This is particularly true when the axial myocardial displacements are large, mostly during peak diastole (e'), and peak atrial (a') or ventricular (s') systoles. On the other hand, the speckle patterns are well preserved when MoCo is taken into consideration, thus enabling motion estimation based on the tracking of these patterns. We here hypothesized that high-frame-rate high-quality echocardiography based on MoCo allows quantification of fast cardiac motions. Speckle-tracking methods are most commonly based on block matching with normalized cross correlation [4], followed by a subpixel refinement. Subpixel fine tuning is a key step when the frame-to-frame displacements are less than that of the pixel size. Three standard methods were tested in this paper.

TABLE I

ACQUISITION AND POSTPROCESSING PARAMETERS FOR THE *In Vitro* AND *In Vivo* EXPERIMENTS WITH THE VERASONICS RESEARCH SCANNER

Parameters	Values
Acquisitions	
Probe central frequency	2.5 MHz
Pulse repetition frequency	4500 Hz
Number of probe elements	64
Angular width of the sector	90°
Tilt angles	[-16 : +16]°
Number of transmits	36
Sampling frequency	5 MHz
Post Processing	
MoCo overlap	75%
B-mode images	500 images/s
STE ensemble	20 images
STE images	500 images/s

The objective of this paper was twofold: 1) show that accurate STE can be obtained from standard block-matching with high-frame-rate echocardiography based on diverging wave imaging and 2) determine which subpixel refinement is most appropriate. STE was first validated *in vitro* in a rotating disk with normal to subnormal myocardial speeds. High-frame-rate STE of the left ventricular myocardium was then produced *in vivo* in 10 healthy volunteers. The *in vivo* data were acquired with a Verasonics research scanner and the local myocardial displacements were determined using speckle tracking with three different algorithms for subpixel refinement. The global longitudinal strain (GLS) was also determined as it is a robust marker of left ventricular systolic function [18]. The GLS waveforms measured by high-frame-rate echocardiography (500 frames/s) were compared against those obtained with a state-of-the-art clinical General Electric GE scanner (80 frames/s) and commercial workstation (EchoPAC, GE).

II. METHOD

A. Motion-Compensated High-Frame-Rate Ultrasound

The ultrasound in-phase and quadrature components (I/Q) signals were acquired with a Verasonics research scanner (V-1-128, Verasonics Inc., Redmond, WA, USA) and a 2.5-MHz cardiac phased-array transducer (ATL P4-2, 64 elements). The acquisition parameters are reported in Table I. To be consistent with [14], we applied series of 36 tilted 90°-wide diverging waves, with virtual sources located behind the probe (maximal distance $=$ 1.1 cm), to generate high-contrast high-resolution images with the MoCo approach during the compounding process. The successive transmit tilt angles (ranged between $-16°$ and 16°) were arranged triangularly (i.e., increasing then decreasing linearly) to sum the main lobes coherently and the side lobes incoherently, as in [14]. An image rate of 500 images/s was reached using a 36-sample sliding window with 75% overlap (PRF/$36\times4 = 4500/36\times4 = 500$ FPS). The MoCo beamforming protocol was similar to that described in [14]: to generate one compound image, the I/Q signals were summed coherently after delay-and-sum and Doppler-based MoCo. Speckles were tracked on the log-compressed real envelopes (containing 256 radial scanlines, with 500 axial samples each). A clinical GE Vivid q scanner was also used

with another 2.5-MHz phased-array transducer (M4S-RS) for the *in vivo* validation (see Section II-D, *In Vivo* Experiments).

B. Speckle-Tracking Echocardiography

STE was achieved by tracking the speckle patterns using block matching with subsequent subpixel refinement. Since the displacement fields were expected to be smooth, with relatively low-spatial step gradients, we tracked the speckles on low-frequency real envelopes (i.e., amplitude of I/Q signals). This I/Q-based approach also had the methodological advantage to be potentially less sensitive to clutter and to halve data amount (by using quadrature sampling) when compared to RF-based tracking. To determine the motion with a one-pixel precision (whose size was half-wavelength $\times$ 0.35°), we first used the standard method based on the normalized cross correlation calculated in the Fourier domain. Postprocessing parameters are reported in Table I. The real-envelope images (before scan conversion) were divided into small regions of interest whose dimension (32×32) corresponded to 1 cm in the radial direction, and 11° in the cross-range direction. We worked with ensembles of 20 consecutive images, under the assumption that the motion remained unchanged during the time of the successive acquisitions (4.4 ms), to calculate the average of 19 cross correlation matrices (ensemble correlation, see [19]). Peak detection of the averaged normalized cross correlation provided the displacements with a pixel precision. Subpixel precision of the displacement estimates was then obtained through three different methods as follows.

1) *Parabolic Peak Fit of the Cross Correlation*: The correlation was assumed to follow a paraboloid about the peak. Three-point stencils were used in the two directions to locate the correlation peak at a subpixel level [19, p. 160]
2) *Phase Correlation Method*: The phase angles of the normalized cross-power spectrum were fit to a plane using a robust linear regression [20, eq. (3)]. The two slopes of the plane provided the two components of the displacement vectors.
3) *Differential Optical Flow*: The Lucas-Kanade method was used to solve the optical flow equations on the real envelopes. The ensemble included in the overdetermined linear system contained 19 image windows. Hanning weights were assigned in the resulting weighted least-squares problem [21, eq. (8)].

The velocity vectors derived from STE were postprocessed with a robust and unsupervised regularizer based on discrete cosine transforms [22]. This smoother was validated in 2-D and 3-D velocity vector fields containing noisy and spurious values [23]. To avoid subjective smoothing, the regularizing parameter was selected automatically by minimizing the generalized cross-validation GCV score [22].

C. In Vitro Experiments

In vitro experiments were carried out in a 10-cm-diameter rotating disk connected to a step motor. The scales of the experiment matched those observed in the echocardiographic apical view: the upper edge was 2 cm far from the probe, and the scan-depth was 15 cm. The acoustic properties of the disk were tissue like, with the following composition: agar 3%, Sigmacell cellulose powder 3%, glycerol 8%, and water. The outer speeds (velocity amplitudes at the circumference) ranged from 1 to 35 cm/s with a 1.1-cm/s step (maximum angular velocity of 7 rad/s with a 0.2 rad/s step). The angular velocities were chosen to replicate tissue speeds of the left myocardium which can reach values up to 30 cm/s in athletes [24]. The STE-derived velocity vectors were compared with the ground-truth velocity vector field given by the radius and the rotational speed of the disk. Absolute velocity errors were calculated both in radial and cross-range directions and normalized by the outer speeds of the disk. The medians of the normalized errors were reported for a given angular velocity.

D. In Vivo Experiments

The aim of this *in vivo* study was to investigate how high-frame-rate STE compared with state-of-the-art clinical echocardiography for assessing global myocardial deformation. An experienced physician acquired apical four-chamber views of the left ventricle with a GE Vivid q scanner (GE Healthcare) and the Verasonics scanner, successively. The 10 healthy volunteers aged 20–40 years were enrolled in the *in vivo* protocol approved by the human ethical review committee of the CRCHUM (Research Center of the University of Montreal Hospital, Montreal, QC, Canada). The GE imaging sequence was a conventional sequential focusing approach at 60–80 frames/s. The Verasonics scanning sequence and the MoCo beamforming approach are described in Section II-A. Since the I/Q signals issued from the diverging waves were beamformed offline, the on-screen display with the Verasonics was of poor quality (no MoCo, low refresh rate). With the Verasonics scanner, the location and orientation of the probe were thus adjusted using a prior sequential focused sequence before switching to the high-frame-rate acquisition. From these 10 pairs (GE + Verasonics) of acquisitions, we computed the GE- and Verasonics-derived GLS. The GLS is a prognostic marker of the global left ventricular systolic function measured clinically by STE from a long-axis apical view [25]. It reflects the relative longitudinal contraction (in percent) of the myocardium. The GLS peak is known to be around -20% in normal subjects [26]. The GE-derived GLS were determined by a physician using an EchoPAC workstation (GE Healthcare) with the proprietary speckle-tracking technique. The Verasonics-derived GLS was measured after STE with the three abovementioned subpixel methods as follows. For a given subject, the endocardium was delineated manually in the first B-mode image of the high-frame-rate series under the supervision of a physician. This sampled contour was tracked automatically, from frame-to-frame, using the three abovementioned subpixel techniques. The instantaneous GLS (in percentage) was estimated as $\mathrm{GLS}(t) = 100[L(t) - \max(L)]/\max(L)$ where $L(t)$ is the longitudinal endocardial length at time t. Note that we used the maximum length of the endocardium instead of its length at end-diastole since we did not acquire the electrocardiogram signal when scanning with the Verasonics. This approximation does not affect GLS significantly in normal patients. The drifts of the strain curves

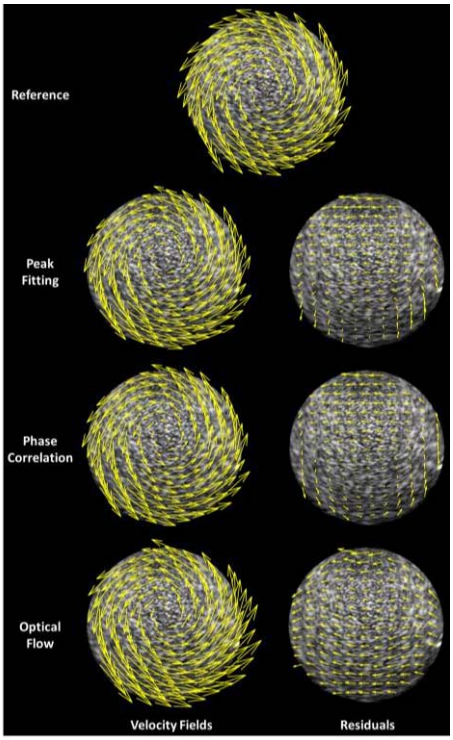

Fig. 1. Examples of estimated *in vitro* velocity fields and the corresponding residuals (right column), when the disk outer speed was 15 cm/s. From top to bottom: 1) theoretical ground truth and velocity fields derived from: 2) correlation peak fitting; 3) phase correlation; and 4) optical flow.

were corrected assuming that the length of the left ventricle should return to its original length after a complete heart cycle. In clinical STE, drift correction is recommended to remove cumulative errors. Drift was corrected by affine regression. The GLS peaks determined by high-frame-rate echocardiography (Verasonics) were compared with those returned by the EchoPAC workstation. The four groups (one GE-derived + three Verasonics-derived) were compared using a multiple pairwise comparison test with the Bonferroni correction (MATLAB, Statistics Toolbox, Mathworks Inc.).

III. Results

A. In Vitro

The velocity vector images of the disk (see Fig. 1) show that STE was able to uncover the rigid rotation, with the three subpixel methods, when MoCo was involved. As a comparison, Fig. 2 illustrates that MoCo was essential for speckle tracking, especially in the presence of large motions.

The estimated velocity fields with MoCo were consistent with the ground-truth fields, but a bias was observed (the center was upward) likely due to the degradation of the cross-range resolution with depth. As shown in Fig. 3, the normalized cross-range errors were higher than the normalized radial errors (lower bound = 10% versus 4%, Fig. 3). The phase correlation performed better than did the other methods *in vitro* (Fig. 3; radial: 4.9% ± 0.7%; and cross-range 12.4% ± 0.7%). When MoCo was not integrated in the compounding process, errors on the velocity estimations reached 45% in the radial

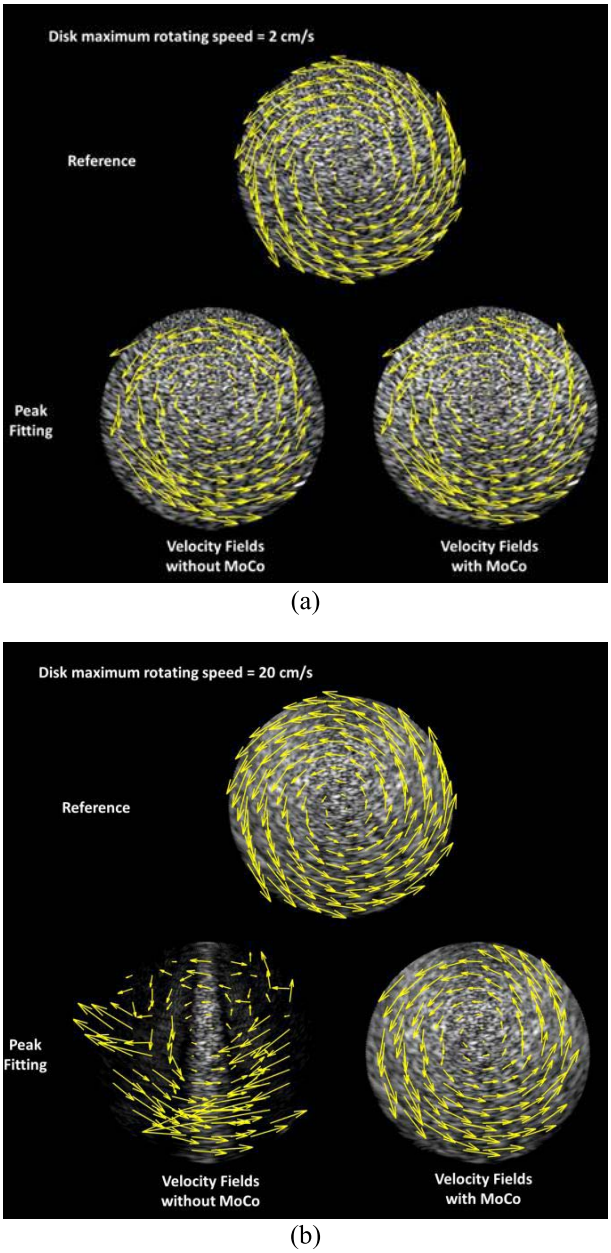

Fig. 2. Examples of estimated velocity fields based on peak fitting, with and without MoCo. The disk outer speeds were (a) 2 and (b) 20 cm/s. In this example, the vectors were not smoothed. Different scales for the velocity vectors were used for a better rendering.

direction when the rotation speed was high, which confirms that MoCo is needed to get high-frame-rate STE. Without MoCo, the speckle patterns were indeed not preserved due to the presence of destructive interferences (see Fig. 2). The optical flow method also returned small errors in the radial direction (5.7% ± 0.8%) but produced the greatest errors in the cross-range direction. The peak fitting approach returned the largest errors in the radial direction, especially when the velocities were small. Peak fitting by interpolation of the cross correlation peak is indeed subject to significant inaccuracy, especially when the frame-to-frame displacements are less than one pixel in magnitude [27]. As a side note, speckle tracking with GE-derived B-mode images, obtained

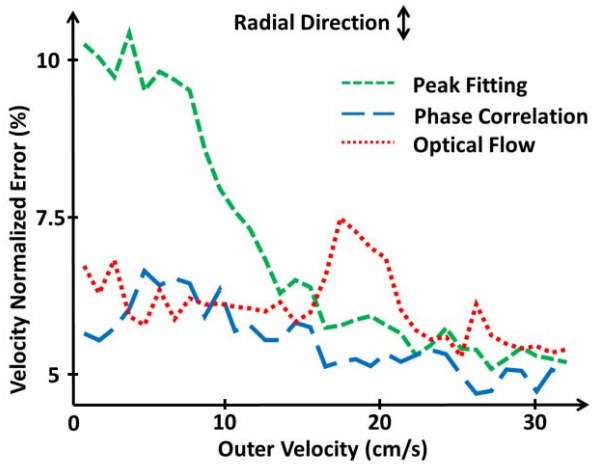

(a)

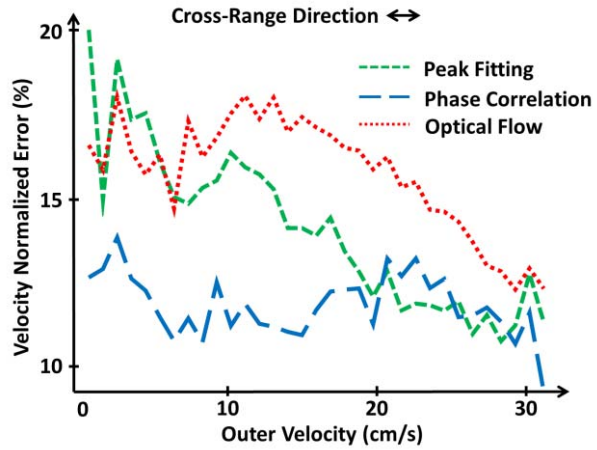

(b)

Fig. 3. *In vitro* normalized errors of the (a) radial and (b) cross-range velocities measured by peak fitting, phase correlation, and optical flow. The abscissa represents the outer speed of the disk.

at maximum frame rate (70 frames/s), failed with the three methods for large motions. The normalized errors in the cross-range direction were between 20% and 50% beyond a rotation speed of 5 rad/s.

B. In Vivo

Fig. 4 shows left ventricular velocity vector images of one volunteer during systole (left column) and diastole (right column). Velocity vectors from peak fitting and optical flow have similar directions, but smaller amplitudes were observed with peak fitting. The phase-based approach failed to detect cardiac motion. These observations were repeated throughout the whole cardiac cycle, as can be seen in the movies of the supplementary content. The GLS waveforms of the same subject are depicted in Fig. 5 and compared with that obtained from the GE scanner and workstation. Consistently, with the velocity vector images of Fig. 4, subpixel refinement with optical flow returned the best match. Peak fitting and phase correlation led to substantial underestimations. This was observed in 10 volunteers, as revealed by the GLS systolic peaks (see Fig. 6). The optical flow and GE methods returned values in the normal range (around -20%), whereas the GLS peaks obtained with peak fitting and phase correlation were in the subnormal range. Although a larger variance was observed in the optical flow method in comparison with GE, their means were not significantly different (p value $=$ 0.33). The other pairwise comparisons indicated significant differences of the means (p value $< 10^{-5}$). The Bland-Altman statistics (Verasonics GLS $-$ GE GLS, mean ± 2 std) were: GE versus 1) peak fitting: $7.2\% \pm 3.6\%$; 2) phase correlation: $14.7\% \pm 4.3\%$; and 3) optical flow: $2.2\% \pm 4.7\%$. These results denote that phase correlation and peak fitting are likely not adapted for *in vivo* high-frame-rate STE.

IV. Discussion

We introduced high-frame-rate STE based on steered diverging waves, MoCo, and speckle tracking by block matching. We obtained STE at 500 frames/s, which is around 6 times higher than in conventional clinical scanners. The *in vitro* study showed that high-tissue velocity amplitudes (up to 30 cm/s) can be measured with our method. The pilot *in vivo* study illustrated that the GLSs determined by high-frame-rate STE in 10 subjects were consistent with those measured with a commercial workstation. At very high frame rates, local frame-to-frame displacements can be very small. Subpixel motion estimation is thus a critical aspect. Three basic different schemes for subpixel refinement in speckle tracking were tested. In our *in vivo* study, a subpixel motion estimator through an optical flow method returned the best outputs. To sum up, this paper demonstrates that:

1) MoCo is a necessary condition for myocardial speckle tracking when coherent compounding is involved.
2) STE of the myocardium is feasible at very high frame rates.
3) Robust algorithms for subpixel motion estimation are of key importance when dealing with *in vivo* data.

These aspects are discussed in the following.

A. Significance of Motion Compensation for Speckle Tracking in High-Frame-Rate Echocardiography

Assessment of the myocardial dynamics by speckle tracking is possible only if the speckle patterns are well preserved, which can be challenging at very high frame rates. Andersen *et al.* [8] have tackled this problem by introducing a multistep tracking method, including spatial and temporal filtering, detection of strong-intensity speckles, constrained feature tracking, and final smoothing. They used a 16:1 parallel receive ("explososcanning," [28]) to obtain long-axis views of the left ventricle at 500 frames/s. This composite-tracking process might have been necessary to deal with the relatively low contrast of their images (no coherent compounding was used). In this original feasibility study, they tested their approach on 10 subjects and confirmed that speckle tracking is possible in high-frame-rate echocardiography. In our study, we obtained wide-sector scans of high-quality images of the four cardiac chambers at 500 frames/s. As explained earlier, axial motion was compensated during coherent compounding

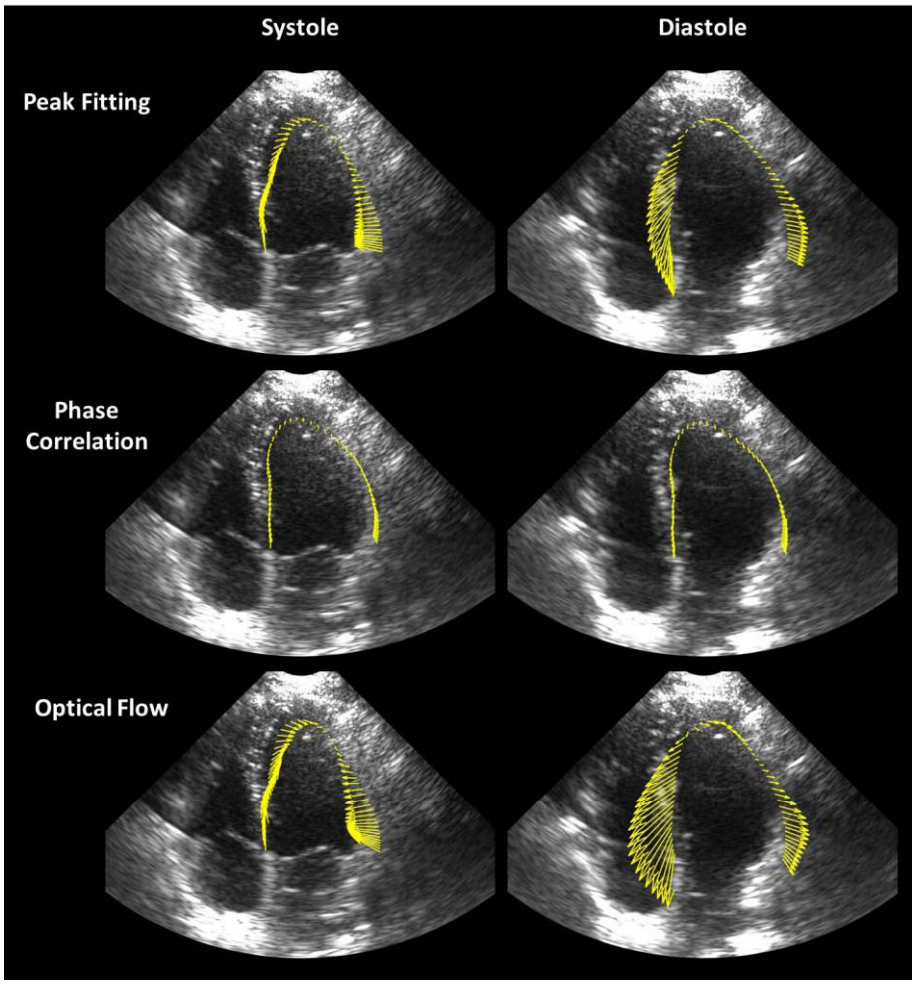

Fig. 4. Systolic (left column) and diastolic (right column) motion fields of the left myocardium in one healthy volunteer. From top to bottom: velocity vector images derived from three different subpixel techniques based on: 1) peak fitting; 2) phase correlation; and 3) optical flow.

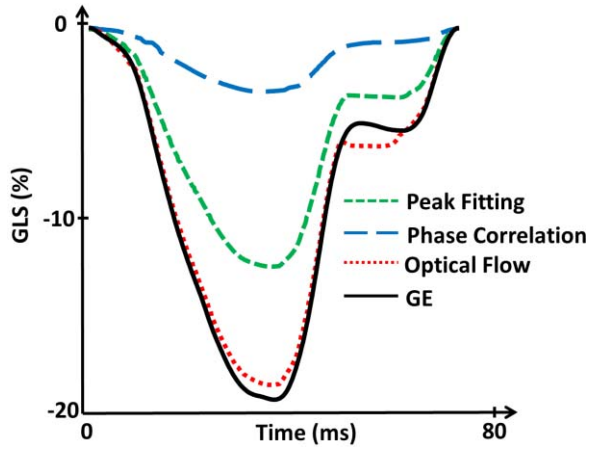

Fig. 5. GLS waveform in one healthy volunteer (same as in Fig. 4). GLS was obtained from motion estimation measured by peak fitting, phase correlation, and optical flow. The GLS provided by the GE clinical scanner is represented as a reference.

to discard the destructive interferences that can be generated by the large movements of the myocardium. To this end, MoCo was carried out using an original method developed by Porée *et al.* [14] and based on tissue Doppler. In the absence of MoCo, significant signal losses were discernible in the B-mode images see [14, Fig. 12], especially during peak diastole and systole, thus making myocardial speckle tracking not viable. In this paper, we demonstrated both *in vitro* and *in vivo* that preservation of the speckle patterns through MoCo allowed accurate cardiac motion estimation at high frame rates with a standard subpixel block-matching algorithm. This was confirmed by the consistent GLS waveforms obtained with the optical-flow motion estimator in 10 volunteers using a Verasonics research scanner. Hence, MoCo is a necessary condition for myocardial speckle tracking when coherent compounding is required. When less (or no) compounding is done, the adverse effect of motion might be less detrimental and might, therefore, have less impact on speckle tracking. It is expected that a compromise must be made in terms of image and tracking quality. With regard to the MLT approach, since it is compounding free [9], [10], MoCo is not needed. It would be of interest to investigate to which extent the receipt cross-talks inherent in MLT may affect speckle tracking.

B. Comparison of the Speckle-Tracking Algorithms

Three basic subpixel block-matching methods were tested, with similar input parameters, both *in vitro* and *in vivo*, i.e.,

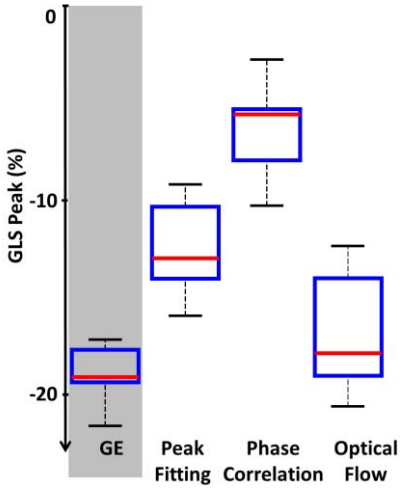

Fig. 6. Distributions of the GLS peaks determined in 10 healthy volunteers by peak fitting, phase correlation, and optical flow. The GLS peak distribution returned by the GE clinical scanner is represented as a reference.

similar subwindow size, ensemble length, and validation. Significant differences were observed between the *in vitro* and *in vivo* findings, leading to contradictory conclusions. The phase-based approach was the most accurate *in vitro*, regardless of the rotation speed. However, it was ineffective *in vivo*. The rotating disk setup provided high-contrast high-SNR B-mode images, was free of out-of-plane motions, and the movements were rigid (no deformation) and steady (no acceleration). These ideal conditions were obviously not met *in vivo*. Furthermore, the *in vivo* images were marred by artifacts classically encountered in medical ultrasound imaging, and mostly related to propagation path and attenuation. These disparities likely explain, in large part, the conflicting results observed in our experiments, especially regarding the phase correlation. Phase-based algorithms are indeed known to be very sensitive to noise [20]. According to our results, it is thus likely that phase-based approaches are poorly adapted for high-frame-rate echocardiography. A number of numerical techniques have been introduced to mitigate the adverse effects of noise for phase correlation with least-squares fitting (see [29], [30]). In our study, however, we only focused on the comparison of three different motion trackers in their most basic form. Note that the transverse oscillation approach, also a phase-based technique, has been successfully validated *in vivo* with large-aperture (linear) arrays [31], [32]. In the same direction, a recent theoretical study described the optimal conditions to estimate the cross-range motion using transverse oscillations in cardiac phased-array imaging [33]. Since their findings were not supported by *in vivo* data, no explicit conclusions can be pronounced regarding the clinical utility. Of note, one *in vivo* case for cardiac motion in echocardiography with transverse oscillations was analyzed by Alessandrini *et al.* [34]. The reported global strain values, however, were much below the normal ranges. Further *in vivo* studies are thus required to check the clinical reliability of this approach. The method based on peak fitting constantly underestimated the displacements both *in vitro* and *in vivo*. This can be explained by the well-documented "peak-locking effect," the tendency of peak fitting to bias toward integral pixel values [35]. In our study, pointwise frame-to-frame displacements were all less than 0.5 pixels in the cross-range direction; the peak-locking effect thus induced a consistent bias toward zero. Although other fitting models exist (paraboloid, Gaussian, centroid, etc.,), they are also all sensitive to the peak-locking effect. In our study, the differential optical flow approach returned the most accurate GLS waveforms in 10 subjects (see Figs. 4 and 5), and they were very consistent with those obtained by the clinical GE scanner and the EchoPAC workstation, although some underestimation and larger variance were noticed. This further confirms that the myocardial speckles were well preserved during diverging wave imaging with MoCo beamforming.

C. Possible Improvements of the Optical Flow Method

The use of high-frame-rate echocardiography allowed us to implement algorithms based on large slow-time ensembles (of length 20): 1) ensemble correlation before peak fitting; 2) ensemble phase correlation; or 3) overdetermined linear systems in the optical flow approach. As already discussed, a differential optical flow method provided the best results. In this paper, we used a local Lucas-Kanade approach in its simplest form (locally rigid translations). Parametric models could be integrated to potentially improve motion estimation, such as those assuming locally affine motions [36]. In particular, this approach has long been used in vascular elastography [37], [38]. Since the myocardial velocity field is smooth, a global regularized method [39] could also increase the robustness of the estimation. In addition, because tissue Doppler is given by the MoCo process, it could be combined with the optical flow measurement in a least-squares regularized problem as in [40]. A supplementary constraint based on tissue Doppler can very likely reduce biases. Finally, the addition of physiological constraints or deformation models [41] could further reduce errors due to out-of-plane motions, for example.

D. Global Longitudinal Strain (GLS)

The GLS waveforms and peaks were concordant with those returned by a clinical ultrasound scanner (Figs. 5 and 6). We choose GLS as clinical index to validate our *in vivo* results since it has become widely accepted in strain imaging for assessing the systolic left ventricular function. Due to significant intervendor variability in strain images, it has been recently reported that GLS is the only myocardial strain parameter which may be safely used in routine clinical practice [42]. It would be of interest to test our approach for determining longitudinal strains locally to offer high-frame-rate strain imaging. This would be particularly relevant for simultaneous strain imaging in all four cardiac chambers, where wide deep sectors are required at the expense of frame rate [43]. High-frame-rate strain imaging can also be of importance in stress echocardiography where heart beats are around 120 bpm. We plan to address these topics in a future study with an MRI-ultrasound-compatible *in vitro* phantom [44] which reproduces myocardial shortening, torsion,

and contraction (lengthening, untwisting, and dilation) during systole (diastole).

E. Volumetric Three-Component STE and Volumetric GLS

To fully characterize cardiac motion and deformation, volumetric three-component velocity vector imaging (STE) will be the logical continuation of this 2-D study. Since its temporal resolution is limited, 3-D echocardiography is currently restricted by the need of stacking several small scan volumes acquired during consecutive heart beats. This limitation makes 3-D STE not clinically compliant since it requires time-demanding acquisitions and supervised postprocessing. High-frame-rate 3-D cardiac imaging will be needed to attain sufficient temporal and spatial resolutions in a single heartbeat. Different potential strategies are worth mentioning: 1) multiplane transmits [45], a generalization of the MLT method; 2) row-column-addressed arrays [46]; 3) 2-D sparse arrays [47]; 4) synthetic aperture imaging with a 1024-element 2-D transducer array [48], [49]. Whether these different procedures adequately preserve the speckle patterns for effective speckle tracking has not been investigated. To obtain high-frame-rate high-quality volumetric echocardiography, we will update our MoCo strategy for 3-D using steered spherical diverging waves.

V. Summary and Conclusion

In this paper, we presented an innovative method based on the combination of MoCo and speckle tracking to perform high-frame-rate STE of the left ventricle. High-frame-rate velocity vector images of the cardiac muscle were generated with three common speckle-tracking approaches for subpixel estimation. Subpixel refinement based on differential optical flow was the most robust in the left ventricle of 10 subjects and allowed accurate high-frame-rate STE. This paper illustrates that coherent compounding with MoCo preserves the speckle patterns and makes it possible to carry out efficient speckle tracking. The 3-D speckle tracking of the myocardium will be the logical follow-up of the present findings.

References

[1] D. Vray *et al.*, "Ultrasound medical imaging," in *Medical Imaging Based on Magnetic Fields and Ultrasounds*, H. Fanet, Ed. Wiley, 2014, pp. 1–72.

[2] H. Geyer *et al.*, "Assessment of myocardial mechanics using speckle tracking echocardiography: Fundamentals and clinical applications," *J. Amer. Soc. Echocardiogr.*, vol. 23, no. 4, pp. 351–369, 2010.

[3] J. Gorcsan, III, and H. Tanaka, "Echocardiographic assessment of myocardial strain," *J. Amer. College Cardiol.*, vol. 58, no. 14, pp. 1401–1413, 2011.

[4] J. D'hooge, "Principles and different techniques for speckle tracking," in *Myocardial Imaging: Tissue Doppler and Speckle Tracking*, T. Marwick, C.-M. Yu, J. P. Sun, Eds. Oxford, U.K.: Blackwell, 2007, pp. 17–25.

[5] J.-U. Voigt *et al.*, "Definitions for a common standard for 2D speckle tracking echocardiography: Consensus document of the EACVI/ASE/Industry Task Force to standardize deformation imaging," *Eur. Heart J. Cardiovascular Imag.*, vol. 16, no. 1, pp. 1–11, 2015.

[6] T. H. Marwick, "Stress echocardiography," *Heart*, vol. 89, no. 1, pp. 113–118, 2003.

[7] M. Cikes, L. Tong, G. R. Sutherland, and J. D'hooge, "Ultrafast cardiac ultrasound imaging: Technical principles, applications, and clinical benefits," *JACC, Cardiovascular Imag.*, vol. 7, no. 8, pp. 812–823, 2014.

[8] M. V. Andersen *et al.*, "High-frame-rate deformation imaging in two dimensions using continuous speckle-feature tracking," *Ultrasound Med. Biol.*, vol. 42, no. 11, pp. 2606–2615, Nov. 2016.

[9] R. Mallart and M. Fink, "Improved imaging rate through simultaneous transmission of several ultrasound beams," *Proc. SPIE*, vol. 1733, pp. 120–130, Nov. 1992.

[10] L. Tong, A. Ramalli, R. Jasaityte, P. Tortoli, and J. D'hooge, "Multi-transmit beam forming for fast cardiac imaging—Experimental validation and *in vivo* application," *IEEE Trans. Med. Imag.*, vol. 33, no. 6, pp. 1205–1219, Jun. 2014.

[11] L. Tong *et al.*, "Wide-angle tissue Doppler imaging at high frame rate using multi-line transmit beamforming: An experimental validation *in vivo*," *IEEE Trans. Med. Imag.*, vol. 35, no. 2, pp. 521–528, Feb. 2016.

[12] H. Hasegawa and H. Kanai, "High-frame-rate echocardiography using diverging transmit beams and parallel receive beamforming," *J. Med. Ultrason.*, vol. 38, no. 3, pp. 129–140, 2011.

[13] C. Papadacci, M. Pernot, M. Couade, M. Fink, and M. Tanter, "High-contrast ultrafast imaging of the heart," *IEEE Trans. Ultrason., Ferroelect., Freq. Control*, vol. 61, no. 2, pp. 288–301, Feb. 2014.

[14] J. Porée, D. Posada, A. Hodzic, F. Tournoux, G. Cloutier, and D. Garcia, "High-frame-rate echocardiography using coherent compounding with Doppler-based motion-compensation," *IEEE Trans. Med. Imag.*, vol. 35, no. 7, pp. 1647–1657, Jul. 2016.

[15] J. Wang and J. Y. Lu, "Motion artifacts of extended high frame rate imaging," *IEEE Trans. Ultrason., Ferroelect., Freq. Control*, vol. 54, no. 7, pp. 1303–1315, Jul. 2007.

[16] B. Denarie *et al.*, "Coherent plane wave compounding for very high frame rate ultrasonography of rapidly moving targets," *IEEE Trans. Med. Imag.*, vol. 32, no. 7, pp. 1265–1276, Jul. 2013.

[17] K. L. Gammelmark and J. A. Jensen, "2-D tissue motion compensation of synthetic transmit aperture images," *IEEE Trans. Ultrason., Ferroelect., Freq. Control*, vol. 61, no. 4, pp. 594–610, Apr. 2014.

[18] S. A. Reisner, P. Lysyansky, Y. Agmon, D. Mutlak, J. Lessick, and Z. Friedman, "Global longitudinal strain: A novel index of left ventricular systolic function," *J. Amer. Soc. Echocardiogr.*, vol. 17, no. 6, pp. 630–633, 2004.

[19] M. Raffel, C. E. Willert, S. Wereley, and J. Kompenhans, "Image evaluation methods for PIV," in *Particle Image Velocimetry: A Practical Guide*, 2nd ed. New York, NY, USA: Springer, 2007, pp. 122–176.

[20] H. Foroosh, J. B. Zerubia, and M. Berthod, "Extension of phase correlation to subpixel registration," *IEEE Trans. Image Process.*, vol. 11, no. 3, pp. 188–200, Mar. 2002.

[21] J. L. Barron, D. J. Fleet, and S. S. Beauchemin, "Performance of optical flow techniques," *Int. J. Comput. Vis.*, vol. 12, no. 1, pp. 43–77, 1994.

[22] D. Garcia, "Robust smoothing of gridded data in one and higher dimensions with missing values," *Comput. Statist. Data Anal.*, vol. 54, no. 4, pp. 1167–1178, Apr. 2010.

[23] D. Garcia, "A fast all-in-one method for automated post-processing of PIV data," *Experim. Fluids*, vol. 50, no. 5, pp. 1247–1259, Oct. 2010.

[24] P. Caso *et al.*, "Pulsed Doppler tissue imaging in endurance athletes: Relation between left ventricular preload and myocardial regional diastolic function," *Amer. J. Cardiol.*, vol. 85, no. 9, pp. 1131–1136, 2000.

[25] K. Kalam, P. Otahal, and T. H. Marwick, "Prognostic implications of global LV dysfunction: A systematic review and meta-analysis of global longitudinal strain and ejection fraction," *Heart*, vol. 100, no. 21, pp. 1673–1680, 2014.

[26] T. Yingchoncharoen, S. Agarwal, Z. B. Popović, and T. H. Marwick, "Normal ranges of left ventricular strain: A meta-analysis," *J. Amer. Soc. Echocardiogr.*, vol. 26, no. 2, pp. 185–191, 2013.

[27] K. T. Christensen, "The influence of peak-locking errors on turbulence statistics computed from PIV ensembles," *Experim. Fluids*, vol. 36, no. 3, pp. 484–497, 2004.

[28] D. P. Shattuck, M. D. Weinshenker, S. W. Smith, and O. T. von Ramm, "Explososcan: A parallel processing technique for high speed ultrasound imaging with linear phased arrays," *J. Acoust. Soc. Amer.*, vol. 75, no. 4, pp. 1273–1282, 1984.

[29] W. S. Hoge, "A subspace identification extension to the phase correlation method," *IEEE Trans. Med. Imag.*, vol. 22, no. 2, pp. 277–280, Feb. 2003.

[30] J. Ren, J. Jiang, and T. Vlachos, "High-accuracy sub-pixel motion estimation from noisy images in Fourier domain," *IEEE Trans. Image Process.*, vol. 19, no. 5, pp. 1379–1384, May 2010.

[31] S. Salles, A. J. Y. Chee, D. Garcia, A. C. H. Yu, D. Vray, and H. Liebgott, "2-D arterial wall motion imaging using ultrafast ultrasound and transverse oscillations," *IEEE Trans. Ultrason., Ferroelect., Freq. Control*, vol. 62, no. 6, pp. 1047–1058, Jun. 2015.

[32] K. L. Hansen *et al.*, "Analysis of systolic backflow and secondary helical blood flow in the ascending aorta using vector flow imaging," *Ultrasound Med. Biol.*, vol. 42, no. 4, pp. 899–908, Apr. 2016.
[33] B. Heyde, N. Bottenus, J. D'hooge, and G. E. Trahey, "Evaluation of the transverse oscillation technique for cardiac phased array imaging: A theoretical study," *IEEE Trans. Ultrason., Ferroelect., Freq. Control*, vol. 64, no. 2, pp. 320–334, Feb. 2017.
[34] M. Alessandrini *et al.*, "A new technique for the estimation of cardiac motion in echocardiography based on transverse oscillations: A preliminary evaluation in silico and a feasibility demonstration *in vivo*," *IEEE Trans. Med. Imag.*, vol. 33, no. 5, pp. 1148–1162, May 2014.
[35] M. R. Cholemari, "Modeling and correction of peak-locking in digital PIV," *Experim. Fluids*, vol. 42, no. 6, pp. 913–922, 2007.
[36] S. X. Ju, M. J. Black, and A. D. Jepson, "Skin and bones: Multi-layer, locally affine, optical flow and regularization with transparency," in *Proc. IEEE Comput. Soc. Conf. Comput. Vis. Pattern Recognit. (CVPR)*, Jun. 1996, pp. 307–314.
[37] R. L. Maurice, J. Fromageau, É. Brusseau, G. Finet, G. Rioufol, and G. Cloutier, "On the potential of the Lagrangian estimator for endovascular ultrasound elastography: *In vivo* human coronary artery study," *Ultrasound Med. Biol.*, vol. 33, no. 8, pp. 1199–1205, 2007.
[38] C. Naim *et al.*, "Characterisation of carotid plaques with ultrasound elastography: Feasibility and correlation with high-resolution magnetic resonance imaging," *Eur. Radiol.*, vol. 23, no. 7, pp. 2030–2041, Jul. 2013.
[39] L. L. Tarnec, F. Destrempes, G. Cloutier, and D. Garcia, "A proof of convergence of the Horn–Schunck optical flow algorithm in arbitrary dimension," *SIAM J. Imag. Sci.*, vol. 7, no. 1, pp. 277–293, 2014.
[40] V. Tavakoli, N. Bhatia, R. A. Longaker, M. F. Stoddard, and A. A. Amini, "Tissue Doppler imaging optical flow (TDIOF): A combined B-mode and tissue Doppler approach for cardiac motion estimation in echocardiographic images," *IEEE Trans. Biomed. Eng.*, vol. 61, no. 8, pp. 2264–2277, Aug. 2014.
[41] S. Queirós, J. L. Vilaça, P. Morais, J. C. Fonseca, J. D'hooge, and D. Barbosa, "Fast left ventricle tracking using localized anatomical affine optical flow," *Int. J. Numer. Methods Biomed. Eng.*, vol. 33, no. 11, p. e2871, 2017, doi: 10.1002/cnm.2871.
[42] K. E. Farsalinos, A. M. Daraban, S. Ünlü, J. D. Thomas, L. P. Badano, and J.-U. Voigt, "Head-to-head comparison of global longitudinal strain measurements among nine different vendors: The EACVI/ASE inter-vendor comparison study," *J. Amer. Soc. Echocardiogr.*, vol. 28, no. 10, pp. 1171.e2–1181.e2, 2015.
[43] K. Addetia *et al.*, "Simultaneous longitudinal strain in all 4 cardiac chambers: A novel method for comprehensive functional assessment of the heart," *Circulat. Cardiovascular Imag.*, vol. 9, no. 3, p. e003895, 2016.
[44] E. Saloux and F. Tournoux, "Heart phantom assembly," WO Patent 2014 201 571 A1, Dec. 24, 2014.
[45] Y. Chen, L. Tong, A. Ortega, J. Luo, and J. D'hooge, "Feasibility of multiplane-transmit beamforming for real-time volumetric cardiac imaging: A simulation study," *IEEE Trans. Ultrason., Ferroelect., Freq. Control*, vol. 64, no. 4, pp. 648–659, Apr. 2017.
[46] T. L. Christiansen, M. F. Rasmussen, J. P. Bagge, L. N. Moesner, J. A. Jensen, and E. V. Thomsen, "3-D imaging using row–column-addressed arrays with integrated apodization—Part II: Transducer fabrication and experimental results," *IEEE Trans. Ultrason., Ferroelect., Freq. Control*, vol. 62, no. 5, pp. 959–971, May 2015.
[47] E. Roux, A. Ramalli, H. Liebgott, C. Cachard, M. C. Robini, and P. Tortoli, "Wideband 2-D array design optimization with fabrication constraints for 3-D US imaging," *IEEE Trans. Ultrason., Ferroelect., Freq. Control*, vol. 64, no. 1, pp. 108–125, Jan. 2017.
[48] M. F. Rasmussen and J. A. Jensen, "Comparison of 3-D synthetic aperture phased-array ultrasound imaging and parallel beamforming," *IEEE Trans. Ultrason., Ferroelect., Freq. Control*, vol. 61, no. 10, pp. 1638–1650, Oct. 2014.
[49] J. Provost *et al.*, "3D ultrafast ultrasound imaging *in vivo*," *Phys. Med. Biol.*, vol. 59, no. 19, p. L1, 2014.

Philippe Joos, photograph and biography not available at the time of publication.

Jonathan Porée, photograph and biography not available at the time of publication.

Hervé Liebgott, photograph and biography not available at the time of publication.

Didier Vray, photograph and biography not available at the time of publication.

Mathilde Baudet, photograph and biography not available at the time of publication.

Julia Faurie, photograph and biography not available at the time of publication.

François Tournoux, photograph and biography not available at the time of publication.

Guy Cloutier, photograph and biography not available at the time of publication.

Barbara Nicolas, photograph and biography not available at the time of publication.

Damien Garcia, photograph and biography not available at the time of publication.